www.sciencemag.org/content/346/6212/963/suppl/DC1

# Supplementary Material for

## Closing the cohesin ring: Structure and function of its Smc3-kleisin interface

Thomas G. Gligoris, Johanna C. Scheinost, Frank Bürmann, Naomi Petela, Kok-Lung Chan, Pelin Uluocak, Frédéric Beckouët, Stephan Gruber, Kim Nasmyth* Jan Löwe*

*Corresponding author. E-mail: kim.nasmyth@bioch.ox.ac.uk (K.M.); jyl@mrc-lmb.cam.ac.uk (J.L.)

Published 21 November 2014, *Science* **346**, 963 (2014)
DOI: 10.1126/science.1256917

**This PDF file includes:**

## Materials and Methods

In vivo photo cross-linking

Site-directed mutagenesis was used to replace each one of the first 142 codon triplets of *S. cerevisiae* Scc1 by an amber codon (TAG) in an episomal vector (YEpLac181-Scc1-HA3). Of the designed replacements ca. 80% were obtained. Substitutions were introduced into yeast cells in combination with an episomal plasmid bearing an amber-codon-recognizing tRNA and a modified tRNA synthetase(*29*) able to load the amber tRNA with the unnatural photoreactive amino-acid *p*-benzoylphenylalanine (bpa, Bachem). Similarly, using YepLac181-Smc3-myc9 and YepLac181-Smc3-HA6 were employed when making substitutions within the Smc3 ATPase head and coiled coil. Wild type versions of Scc1 and/or Smc3 were counter selected on 5-FOA plates (supplemented with 1-3 mM bpa), and strains assessed for viability and dependence to grow on bpa. For UV-induced cross-linking experiments, cells were grown to log phase in rich medium supplemented with 1 mM bpa and approximately 10 $OD_{600nm}$ units re-suspended in 1 ml ice cold PBS and irradiated with UV light (365nm) for 3x5 min in a Spectrolinker device (Spectroline, total energy of ca. $5.3x10^6$ μJ/$cm^2$). Total protein extraction followed using the standard glass bead TCA method. 25 μg of total protein per sample were analyzed by SDS-PAGE and Western blotting.

Cyanogen bromide chemical cleavage

Photo cross-linking was performed as described above. Strains were grown in YEPD at 30 °C to $OD_{600nm}$ = 1 in cultures supplemented with 1 mM bpa. Cells were broken in 500 μl EBX lysis buffer (50 mM HEPES pH8.0, 100 mM KCl, 2.5 mM $MgCl_2$, 0.05% NP40, 0.25% Triton-X) containing 1 mM DTT, DNase I (1:1,000), Roche Complete Protease Inhibitors (2X) and PMSF (1 mM), lysed in a FastPrep-24 (MP Biomedicals) for 2x1 min at 6 m/s with 500 μl of acid-washed glass beads (425-600 μm, Sigma) and lysates cleared (15 min, 15 k*g*). Immuno-precipitations against myc9-Scc1 were performed using anti-myc antibody (9E10) and protein G sepharose (Amersham Biosciences) at 4 $^oC$ for 1.5 hrs. Immuno-precipitated complexes on beads (30 μl) were treated with 1-2 crystals of CNBr in 70 μl of formic acid. Samples were left incubating overnight at room temperature. After cleavage, water was added to a final volume of 1000 μl, BSA was added to a final concentration of 0.1 mg/ml to improve yield of recovered protein after TCA precipitation (TCA final concentration 10%). Protein was pelleted and washed with ice cold 50 mM Tris/HCl in 80% acetone. Pellets were suspended in SDS loading buffer and loaded onto 15% Tris-glycine gels before Western blotting.

In vivo chemical cross-linking

Strains were grown in YEPD at 30 °C to $OD_{600nm}$ = 0.8 and arrested in nocodazole for 1.5 h. 60 OD units were washed in ice-cold PBS, then re-suspended in 1 ml ice-cold PBS. The suspensions were then split into 2 x 600 μl and 25 μl BMOE (stock: 125 mM in DMSO, 5 mM final) or DMSO was added for 6 min on ice. Cells were washed with 2 x 2 ml ice-cold PBS containing 5 mM DTT, resuspended in 500 μl EBX lysis buffer

containing 1 mM DTT, benzonase (1:1000), RNase (0.1 mg/ml), Roche Complete Protease Inhibitors (2X) and PMSF (1 mM), lysed in a FastPrep-24 (MP Biomedicals) for 3 min at 6 m/s with 500 µl of acid-washed glass beads (425-600 µm, Sigma) and lysates cleared (5 min, 12 k*g*). Protein concentrations were adjusted after Bradford assay and cohesin immuno-precipitated using anti-PK antibody (AbD Serotec, 1 h, 4 °C) and protein G dynabeads (1 h, 4 °C with rotation) in the presence of Halo-TMR substrate (5 µM). Beads were washed with 2 x 1 ml lysis buffer, resuspended in 50 µl 2x sample buffer, incubated at 95°C for 5 min and 40 µl supernatant loaded onto a 5% SDS-PAGE gel. TMR fluorescence was detected on a Fuji FLA-7000 instrument using Cy3 presets. For Western blotting, 5 µl were separated on 3-8% Tris-acetate gels, blotted by semi-dry transfer, probed with anti-myc (Santa Cruz) or anti-PK (AbD Serotec) antibodies and visualized on a LI-COR Odyssey Fc. For Southern blotting, pull-downs of lysates (in 25 mM Hepes pH 8.0, 50 mM KCl, 50 mM $MgSO_4$, 10 mM trisodium citrate, 25 mM sodium sulfite, 0.25% triton-X, Roche Protease Inhibitor, 1 mM PMSF, 2 mM DTT, 0.1 mg/ml RNase) containing a circular 2.3 kb mini-chromosome were performed as above, DNA was eluted in 30 µl 1% SDS with DNA loading dye (65 °C, 4 min) and run on 0.8% agarose gels containing ethidium bromide (1.4 V/cm, 22h, 4 °C).

In vitro chemical cross-linking

Yeast cells from 100 ml YEPD cultures were harvested by centrifugation at $OD_{600}$ = 0.6. Cells were resuspended in 500 µl EBX lysis buffer with 1 mM DTT, 0.5 mM PMSF in isopropanol, 0.1% DNaseI, 1 complete EDTA-free protease inhibitor cocktail tablet (Roche Diagnostics) per 50 ml solution). 500 µl of acid-washed glass beads (425-600 µm, Sigma) were added to the suspension and the cells lysed in a FastPrep-24 instrument (MP Biomedicals) for 2 min at 4.5 m/s. Lysates were spun down for 5 min at 4 °C, 15,000 x*g*, the supernatant removed from the beads and incubated with 100 µl anti-HA sepharose beads (GE Healthcare) for 1.5 h at 4 °C or with 100 µl 9E10 anti-myc serum for 1h at 4 °C and 100 µl of protein G sepharose beads (GE Healthcare) for a further 30 min at 4 °C. The beads were isolated by gentle centrifugation, washed once in lysis buffer (without DTT) before cross-linking. bBBr was added to a final concentration of 0.13 mM and the samples were incubated at 4°C for 10 min. The supernatant was removed, the pellet resuspended in 100 µl 2× SDS loading buffer and the suspension was denaturated at 95 °C for 10 min. Samples were spun down for 5 min at 15,000 x*g* and 5 or 15 µl of the supernatant ran on a 3-8% Tris-acetate gel at 45 mA/gel for 70 min, followed by Western blotting and immuno-detection of the HA or myc epitopes.

Co-expression of Smc3hdCC and Scc1 in *E. coli* and purification of the Smc3-Scc1 complex

A pET28a based plasmid with a version of Smc3NBD and a large part of the emerging coiled coil (Smc3hdCC = $MAY_2$-$S_{260}$linker$D_{971}$-$V_{1230}$StrpII) was co-expressed in BL21(DE3)RIPL *E. coli* with a pET21d-based plasmid of Scc1 (Scc1-N = $M_1$-$N_{115}$-6xHIS). Cells were grown at 37°C to $OD_{600nm}$ = 1, temperature was shifted and when reached 16 °C expression was induced by adding IPTG to a final concentration of 1 mM. Cell pellets were resuspended in $TEN_{150}$ buffer (50 mM Tris pH 7.5, 2 mM EDTA, 150 mM NaCl supplemented with 1 EDTA-free Roche protease inhibitor cocktail tablet per

50 ml) and suspensions passed through a French press at 20 kpsi at 4°C, supplemented with 1 mM PMSF, sonicated on ice, and spun for 1.5 hrs at ~25,000 *g*. The clarified extract was first passed through a Strep-Tactin column (IBA) , the column washed ($TN_{200}$), protein was eluted with desthiobiotin and the eluate was passed through a TALON column (Clontech). After loading the column was washed ($TN_{200}$ with 10 mM imidazole) and captured protein was eluted with 0.5 M imidazole, concentrated in Vivaspin columns (30 kDa cut-off, Vivaproducts) and loaded onto a 16/600 Superdex 200 gel filtration column (GE Healthcare) in 50 mM Tris pH 7.5, 150 mM NaCl, 1 mM βME. For the experiment in panel Fig. S4F, a modified version of Smc3hdCC with a Flag tag was used. After elution and gel filtration, protein was concentrated with Vivaspin columns and crosslinking was performed using bBBr at a final concentration of 0.25 mM for 15 mins on ice.

Yeast live-cell imaging

All strains used for live-cell imaging are diploid. Exponentially growing cells in YEP medium plus 10% glucose were placed on 2.5% agarose pads. Live cell imaging was performed under a spinning disk confocal system (PerkinElmer UltraVIEW) with an EMCCD camera (Hamamatsu) mounted on an Olympus IX8 microscope with Olympus 100x 1.35 NA objectives. Image acquisition was done at room temperature. Seventeen Z-stack images with 0.2 μm intervals were acquired and deconvoluted with Volocity software. Fresh samples were prepared every 10 minutes.

Sucrose gradients and minichromosome separation in SDS-agarose gels

These experiments were performed as described previously (9, 30).

Crystallization, data collection and structure determination

Crystallization conditions were found using LMB's in-house nanolitre crystallization facility (*31*). Crystals were grown by vapor diffusion, equilibrating drops of 100 nl reservoir plus 100 nl protein solution (30 mg/ml in 50 mM Tris pH 7.5, 150 mM NaCl, 1 mM βME, 1 mM ATPγS, 2 mM $MgSO_4$) against reservoirs containing 100 mM imidazole/HCl pH 7.0 and 0.5-1 % (w/v) PEG 200 (vapor diffusion dilutes sample, salting-incrystallization). Crystals were cryo-protected by adding reservoir solution supplemented with 50-60 % (w/v) PEG 200, before flash freezing in liquid nitrogen. Datasets were collected at Diamond Light Source (Harwell, UK) beamlines I24, I02 and I03 on Pilatus detectors and indexed and integrated with XDS (*32*). Data reduction was performed with SCALA(*33*). Molecular replacement with various sequence-related Smc head domains and PHASER (*34*) produced weak hits that were verified to be correct because of ABC ATPase dimer formation. The resulting electron densities were unbuildable so additional phase information was obtained with a SAD experiment on SeMet substituted crystals that were grown under identical conditions. Most selenium sites were found by cross-phasing anomalous differences with the molecular replacement phases and all phase information was then used in order to obtain an electron density map at 3.3 Å resolution, which was of good to adequate quality. The model was manually built and adjusted using MAIN (*35*) and refined with REFMAC (*36*). However, the residue assignment on helices α1 and α2 of Scc1 remained uncertain because of poor

density for the loop between α2 and α3 and a lack of SeMet residues in that area. We therefore verified our model by introducing the mutation K52M into Scc1's α2 and repeated the SAD experiment, which after phasing of the anomalous differences showed a peak at the correct position. The structure and structure factors have been deposited in the Protein Data Bank (PDB) with accession code 4UX3 and statistics of the data and model are summarized in Table 1.

## Supplementary Figures S1-S7

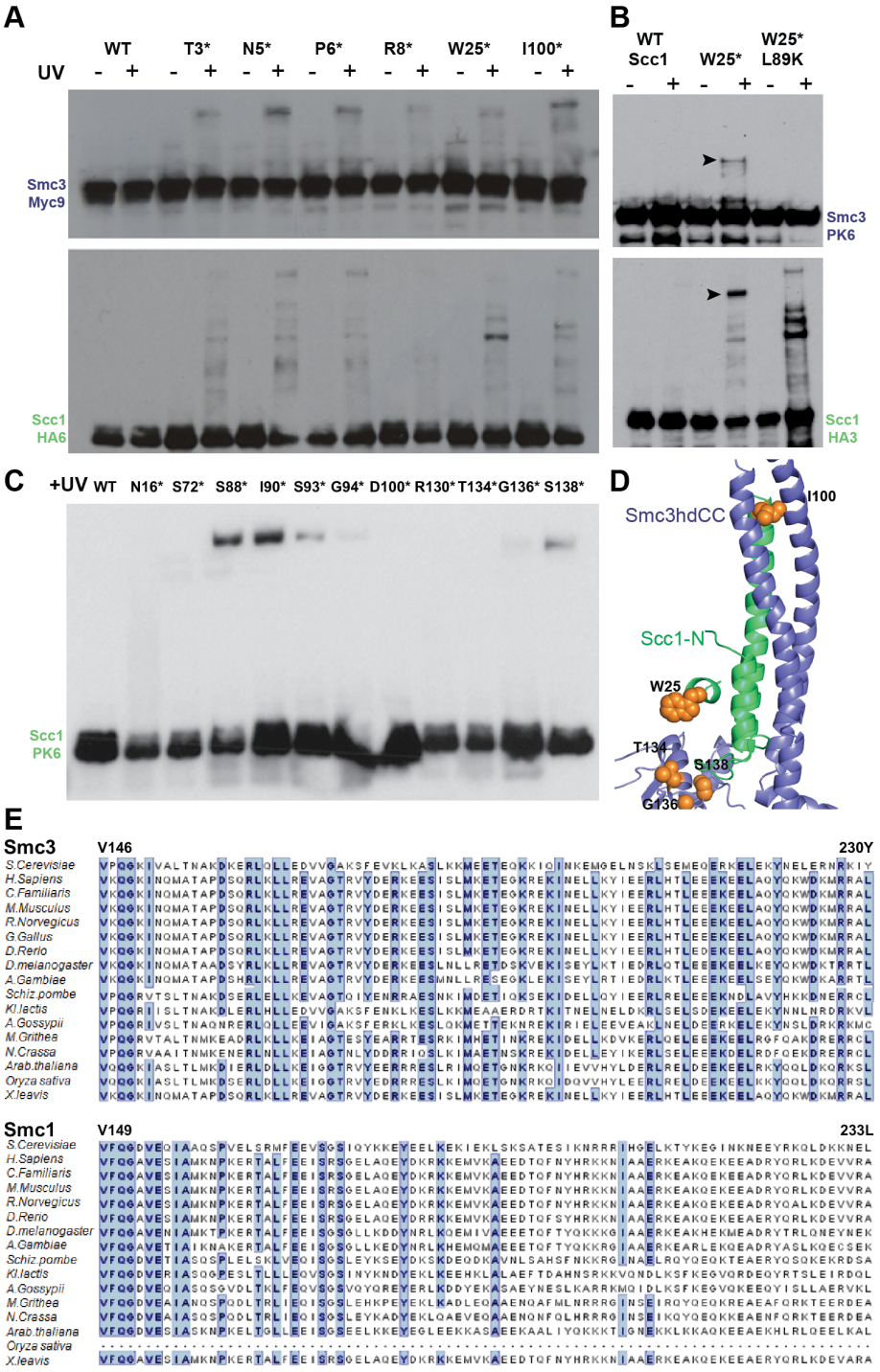

**Figure S1**. In vivo photo cross-linking shows that Scc1's NTD binds Smc3.
We investigated the Smc3/kleisin interaction by in vivo photo cross-linking (*7*), using an orthogonal tRNA and tRNA synthetase pair to incorporate the photoreactive amino acid *p*-benzoyl-phenylalanine (bpa) at nonsense codons at each one of Scc1's N-terminal 142 codons (*7*). Several substitutions by bpa facilitated cross-linking with Smc3 upon UV irradiation of live yeast cells

(A) Western blotting after TCA protein precipitation of yeast strains bearing bpa replacements in Scc1 (T3, N5, P6, W25 and I100 in Scc1). Scc1-PK6 band shifts corresponding to cross-linked species are UV-dependent and contain Smc3.

(B) Scc1W25bpa UV-induced cross-linking as measured by Western blotting following immuno-precipitation of Scc1-HA3 is abolished by Scc1L89K (*11*)

(C) UV-induced cross-links between Scc1 and bpa replacing S88, I90, S93, G136, and S138 within Smc3's ATPase head.

(D) Bpa substitutions (orange spheres) giving rise to moderate UV-dependent cross-linking, located on the Smc3-kleisin structure.

(E) CLUSTALW alignment of the Smc3 and Smc1 amino-terminal sequences from various species highlighting identical residues in blue.

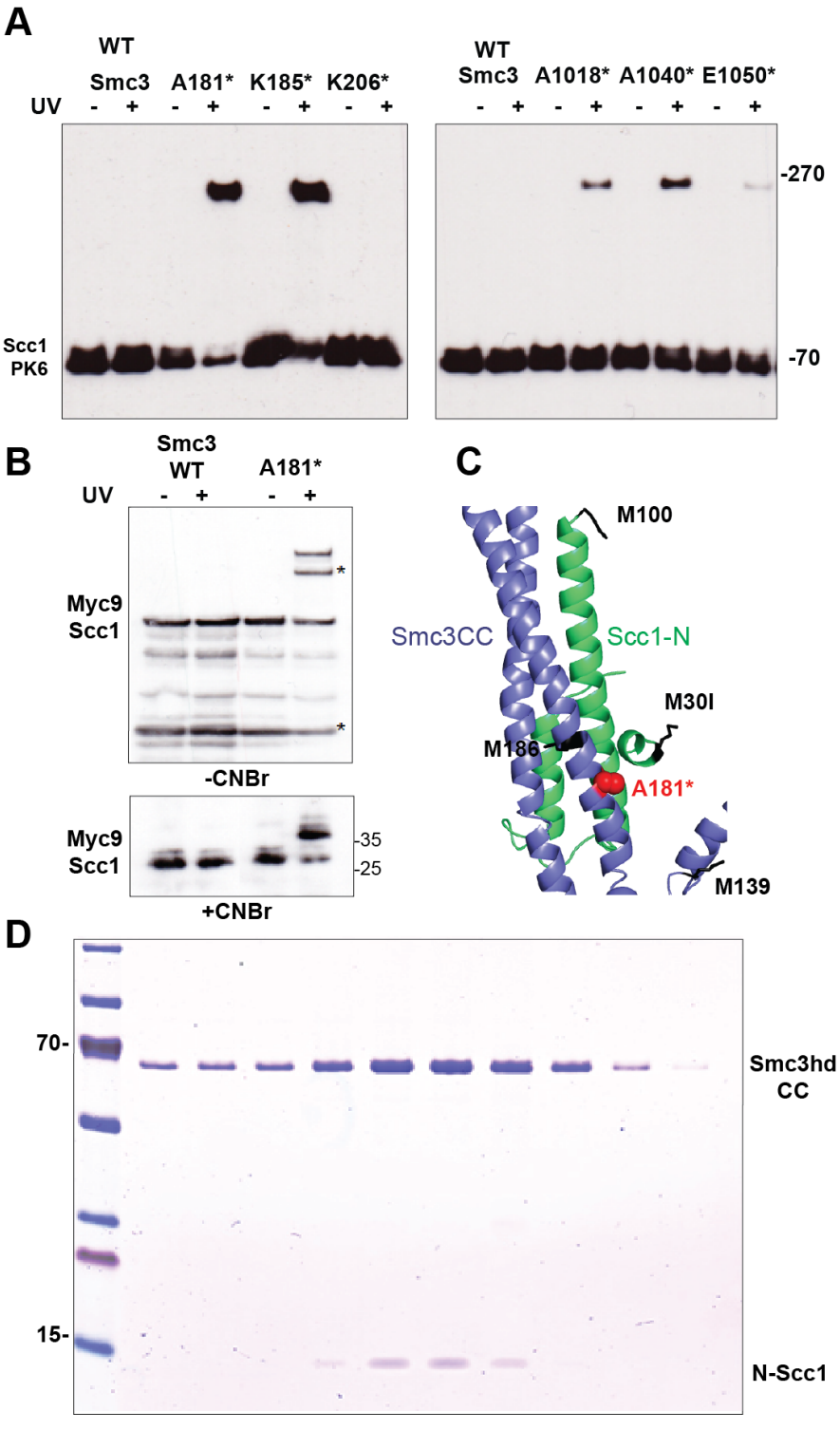
A
WT
Smc3
A181*
K185*
K206*
UV
WT
Smc3
A1018*
A1040*
E1050*
-270
-70
Scc1
PK6
B
Smc3
WT
A181*
UV
Myc9
Scc1
-CNBr
Myc9
Scc1
-35
-25
+CNBr
C
M100
Smc3CC
Scc1-N
M30I
M186
A181*
M139
D
70-
15-
Smc3hd
CC
N-Scc1

**Figure S2.** Scc1's NTD interacts with Smc3's coiled coil in vivo and in vitro.

(A) Immuno-precipitation of Smc3-HA6 after UV irradiation of live cells, followed by Western blotting against Scc1-PK6. Smc3 substitutions A181bpa, K185bpa, A1018bpa, A1040bpa, and E1050bpa but not K206bpa show low to high efficiency photo-crosslinking towards Scc1-PK6. Strains K20358-K20364.

(B) Immuno-precipitation of myc9-Scc1 after UV irradiation of live cells bearing Smc3 with A181bpa. Separase's cleavage fragment and the corresponding upshifted Smc3 cross-linked bands are indicated with an asterisk. Lower panel: cyanogen bromide (CNBr) induced cleavage after methionines creates a shift corresponding to the endogenous fragment flanking M139 and M186 in Smc3 (K20366, K20367).

(C) Ribbon diagram presenting the fragments generated by the CNBr methionine proximal cleavage described in panel (B). Scc1's endogenous M1 has been deleted, an N-terminal myc9 epitope was fused in frame and endogenous M30 was changed to I30. Endogenous Scc1M102, Smc3M139 and M186 generate a 30 kDa Scc1 and a 5 kDa Smc3 fragment. Smc3 cleavage with CNBr creates no other 5 kDa predicted fragment which could contain the cross-linking residue Smc3A181bpa.

(D) A complex containing the first 115 N-terminal residues of Scc1 and the Smc3 ATPase head along with a segment of its coiled coil was purified from a BL21(DE3)RIPL *E. coli* derived strain (TGBL203) and characterized by gel filtration. Proteins visualized by Coomassie staining following SDS-PAGE.

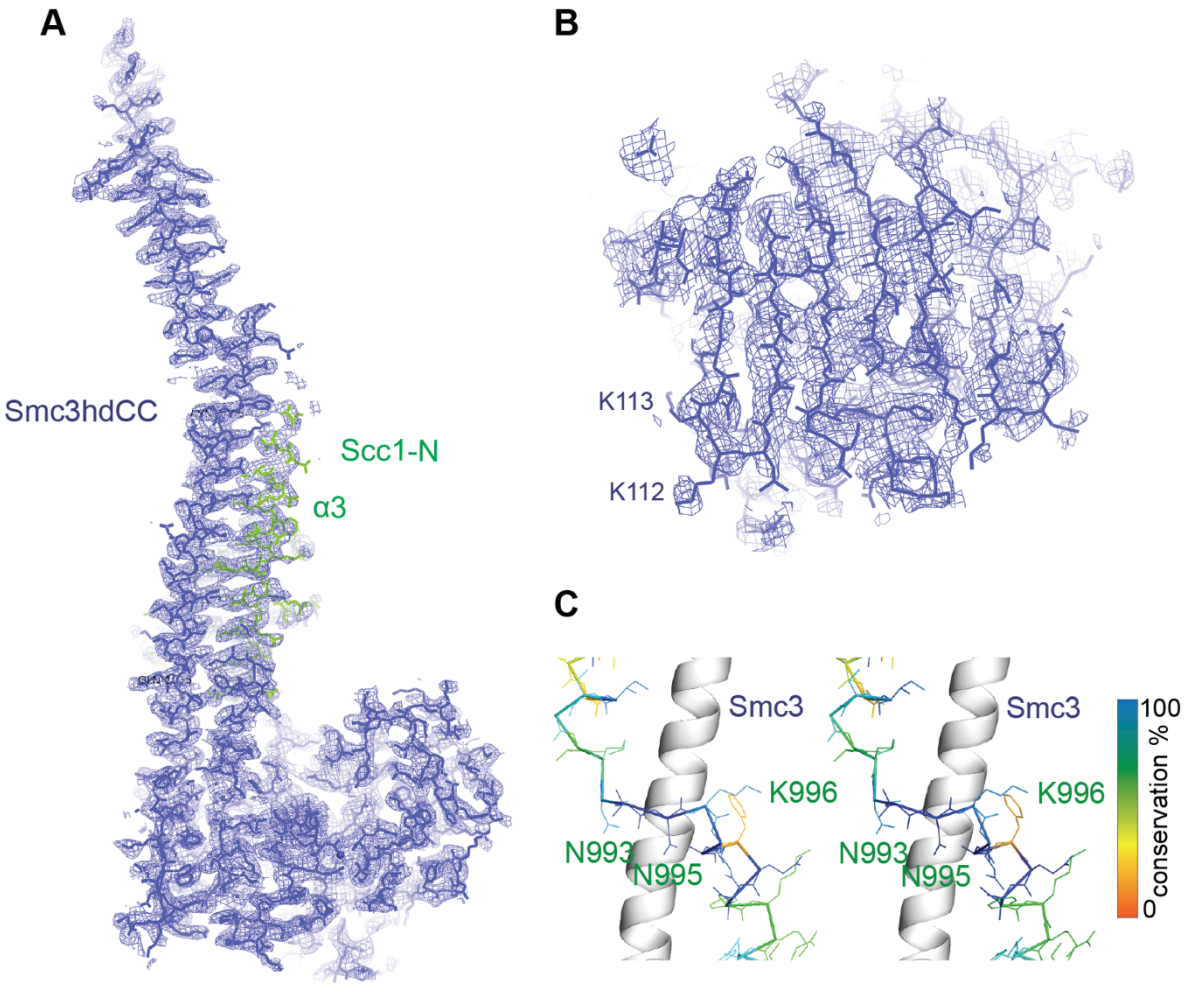


**Figure S3.** Details of the Smc3/kleisin structure.

(A) 2Fo-Fc electron density maps of the Smc3 (Smc3hdCC) and Scc1-N complex with Scc1-N helix α3 highlighted (green).

(B) 2Fo-Fc electron density map of the KKD strand area of the ATPase head. The electron density of the Smc ATPase's beta sheet has lower quality compared to the rest of the structure.

(C) Stereo view of the pronounced conserved kink of the Smc3 coiled coil.

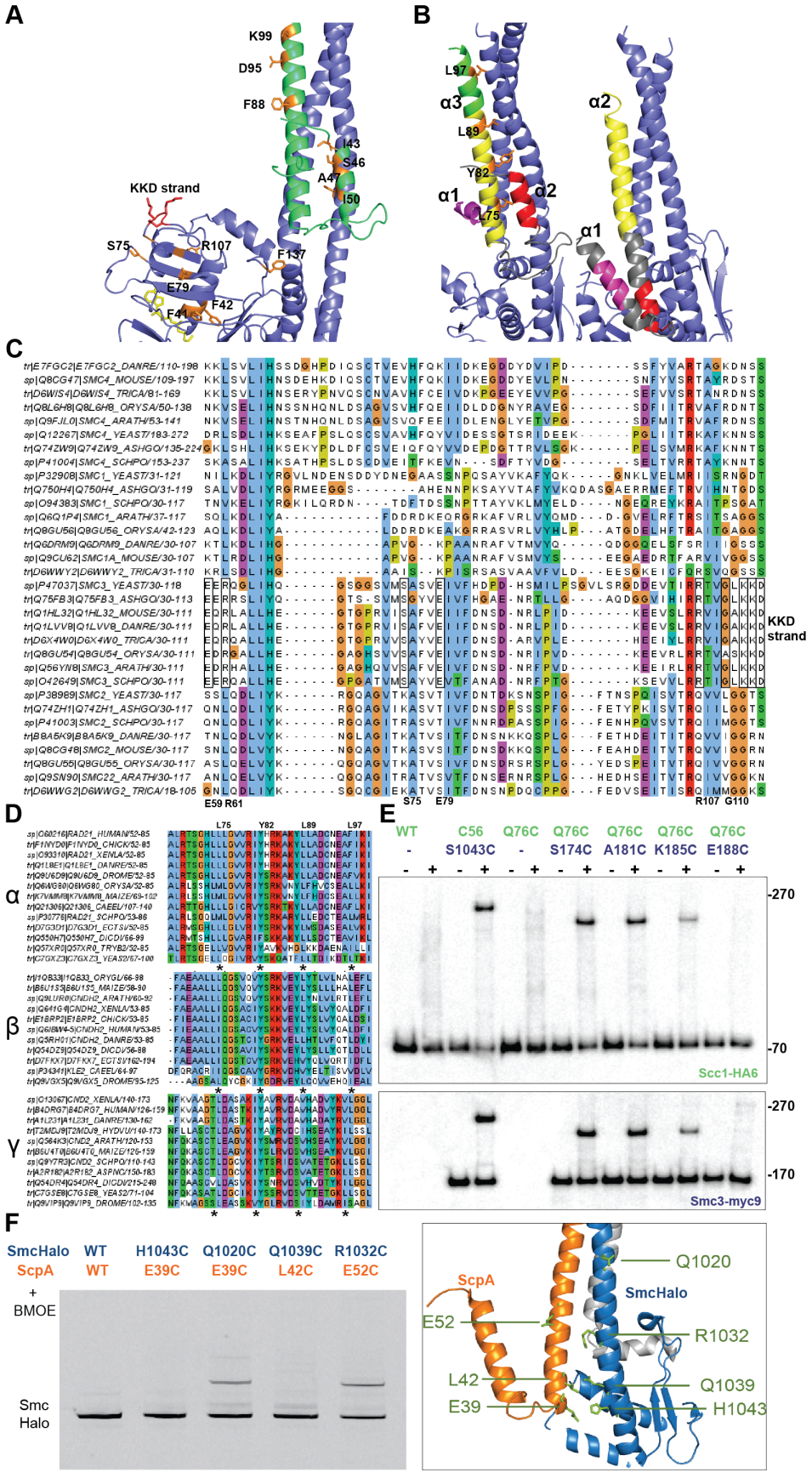
A
K99
D95
F88
I43
S46
A47
I50
KKD strand
S75
R107
F137
E79
F41
F42
B
L97
α3
L89
α2
Y82
α1
L75
α2
α1
C
KKD strand
E59 R61
S75 E79
R107 G110
D
L75 Y82 L89 L97
α
β
γ
E
WT
C56 S1043C
Q76C -
Q76C S174C
Q76C A181C
Q76C K185C
Q76C E188C
- + - + - + - + - + - + - +
-270
-70
Scc1-HA6
-270
-170
Smc3-myc9
F
SmcHalo WT H1043C Q1020C Q1039C R1032C
ScpA WT E39C E39C L42C E52C
+ BMOE
Smc
Halo
ScpA
SmcHalo
Q1020
E52
R1032
L42
Q1039
E39
H1043

**Figure S4.** Conservation of the Smc3 ATPase head and its interface with Scc1.

(A) The KKD strand (red) is distant from the Smc3-kleisin interface. Conserved Smc3-specific residues (F41, F42, S75, E79, R107 and F137) in the ATPase head are highlighted. Amongst these, S75R and R107I/S suppress *eco1*Δ (*15*). Scc1I43, S46, A47, and I50 are conserved and implicated in formation of the four helix bundle with Smc3's coiled coil. F88, D95 and D99, which face away from Smc3 are also highly conserved in α-kleisins.

(B) The three Scc1-N helices and corresponding residues in bacterial *B. subtilis* ScpA are colored, highlighting similarities and differences between the Smc-ScpA (*8*) and Smc3-kleisin structures.

(C) CLUSTALW alignment of Smc1, 2, 3, and 4 ATPase sequences N-terminal to Smc3's KKD strand, showing residues that are highly conserved and Smc3-specific (boxed).

(D) CLUSTALW alignment of the α3 region of α-, β-, and γ-kleisins from a diverse range of species. Residues corresponding to Scc1's L75, Y82, L89, and L97 are conserved in β- and γ- kleisins.

(E) Specificity of the thiol-specific crosslinking assay. Immuno-precipitations against Scc1-HA6 followed by in vitro cross-linking (bBBr) and Western blotting. The Scc1 Q76C substitution cross-links well with Smc3S174C and Smc3A181C, faintly with Smc3K185C and the cross-link is totally lost with Smc3E188C (Strains K18806, K19447, K19579, K19724, K19727, K19728).

(F) The Smc-ScpA complex of *B. subtilis* likely also adopts a four-helix bundle in vivo. Cysteine pairs ScpAE39C-SmcH1043C and ScpAL42C-Q1039C expected to cross link based on the *B. subtilis* structure do not cross-link using BMOE whereas the ScpAE39C-Q1020C pair designed based on the Scc1 Smc3 interface does so (not predicted to cross-link according to the *B. subtilis* structure, PDB 3ZGX). The R1032C-E52C cross-linking indicates the end of the lower part of the respective α3 helix of ScpA. The Smc-ScpA complex as determined from the crystal structure (PDB 3ZGX, panel to the right) is most likely distorted because of crystal packing artifacts.

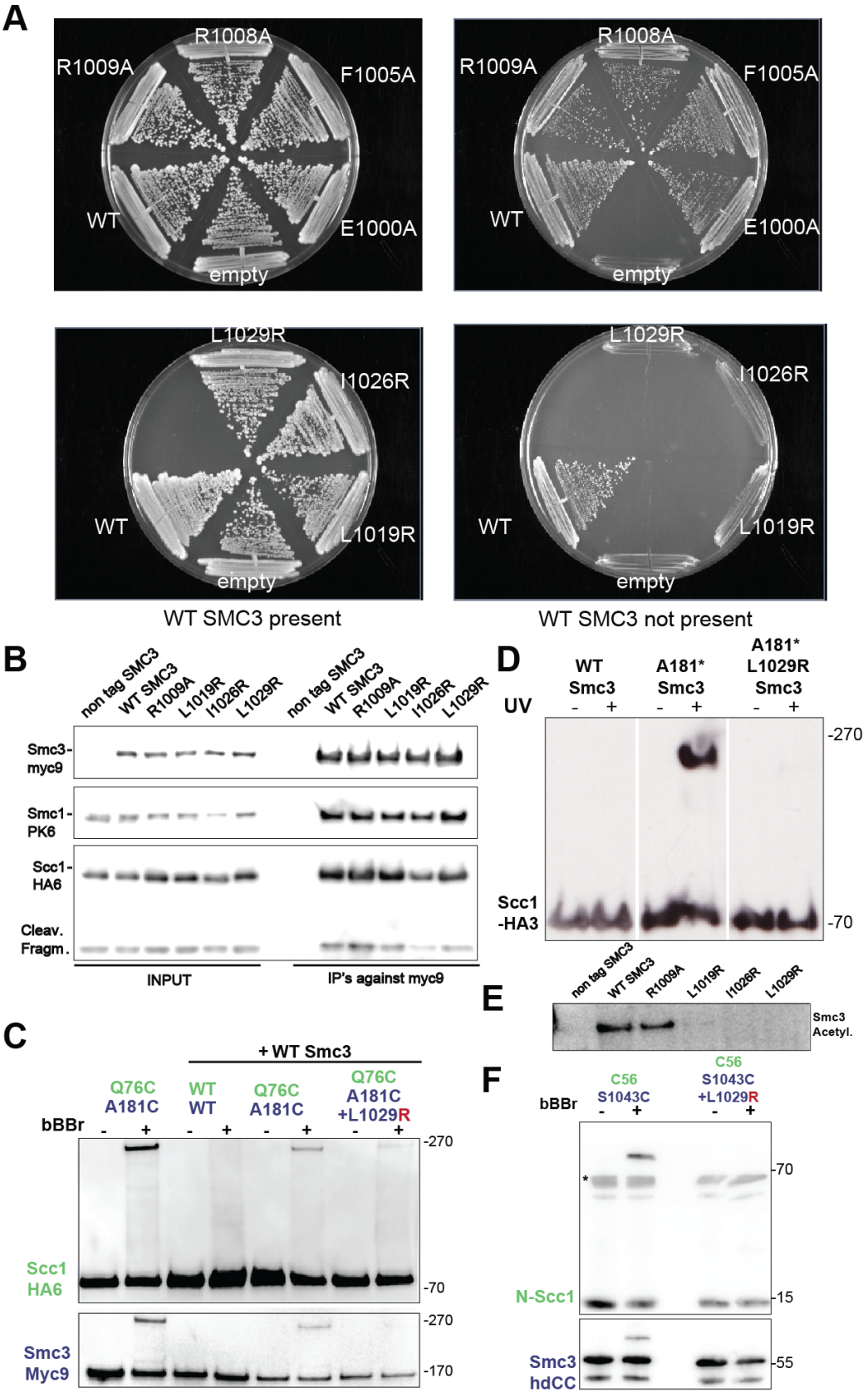
A
R1008A
R1009A
F1005A
WT
E1000A
empty
L1029R
I1026R
L1019R
WT SMC3 present
WT SMC3 not present
B
non tag SMC3
WT SMC3
R1009A
L1019R
I1026R
L1029R
Smc3-myc9
Smc1-PK6
Scc1-HA6
Cleav. Fragm.
INPUT
IP's against myc9
C
+ WT Smc3
Q76C A181C
WT WT
Q76C A181C
Q76C A181C +L1029R
bBBr
Scc1 HA6
Smc3 Myc9
-270
-70
-170
D
WT Smc3
A181* Smc3
A181* L1029R Smc3
UV
Scc1 -HA3
E
Smc3 Acetyl.
F
C56 S1043C
C56 S1043C +L1029R
N-Scc1
Smc3 hdCC
-15
-55

**Figure S5.** Functional analysis of the Smc3-kleisin interface.

(A) Ectopic copies of Smc3L1019R, I1026R and L1029R fail to support growth on 5-FOA plates, which select for loss of a wild type Smc3 gene carried on a centromeric plasmid. In contrast, Smc3E1000A, F1005A, R1008A, and R1009A, which are not predicted to disrupt the Smc3-kleisin interface, support growth (K23121-K23127).

(B) Immuno-precipitations of Scc1-HA6 followed by Western blotting of Scc1-HA6, Smc3-myc9 and Smc1-PK6 shows that cohesin containing Smc3L1019R, I1026R and L1029R still form complexes with Smc1 and Scc1. Scc1-HA6 presumably co-precipitates with Smc3-myc9 due to the unaffected Smc1-kleisin interface (K23147-52).

(C) Strains containing the A181C-Q76 cysteine pair, with or without Smc3L1029R, were used to immuno-precipitate Scc1-HA6 and subjected to bBBr crosslinking followed by Western blotting against Smc3-myc9 and Scc1-HA3 (K20355-57).

(D) Smc3L1029R also disrupts cross-linking induced by Smc3A181bpa. UV-irradiated cells bearing WT Smc3, Smc3A181bpa or Smc3A181bpa L1029R were used to immuno-precipitate Smc3-myc9 followed by Western blotting against Scc1-HA3 (K23153-5).

(E) Smc3 L1019R, I1026R and L1029R but not R1009A abolish K113 acetylation. Immuno-precipitations of Scc1-HA6 followed by Western blotting using anti-acetyl K113 of Smc3 (K23147-52).

(F) L1029R disrupts the Smc3-kleisin interface within complexes produced by *E. coli* in vitro but does not destroy the complex per se. Purified NScc1(6xHIS)-Smc3hdCC(StrpII) complex bearing the L1029R mutation, was precipitated using resin against Smc3Flag followed by gel filtration and then subjected to bBBr crosslinking followed by Western blotting of both Smc3hdCC and Scc1. When L1029R is present the C56-S1043C specific cross-linking is completely abolished. The asterisk denotes a non-specific band.

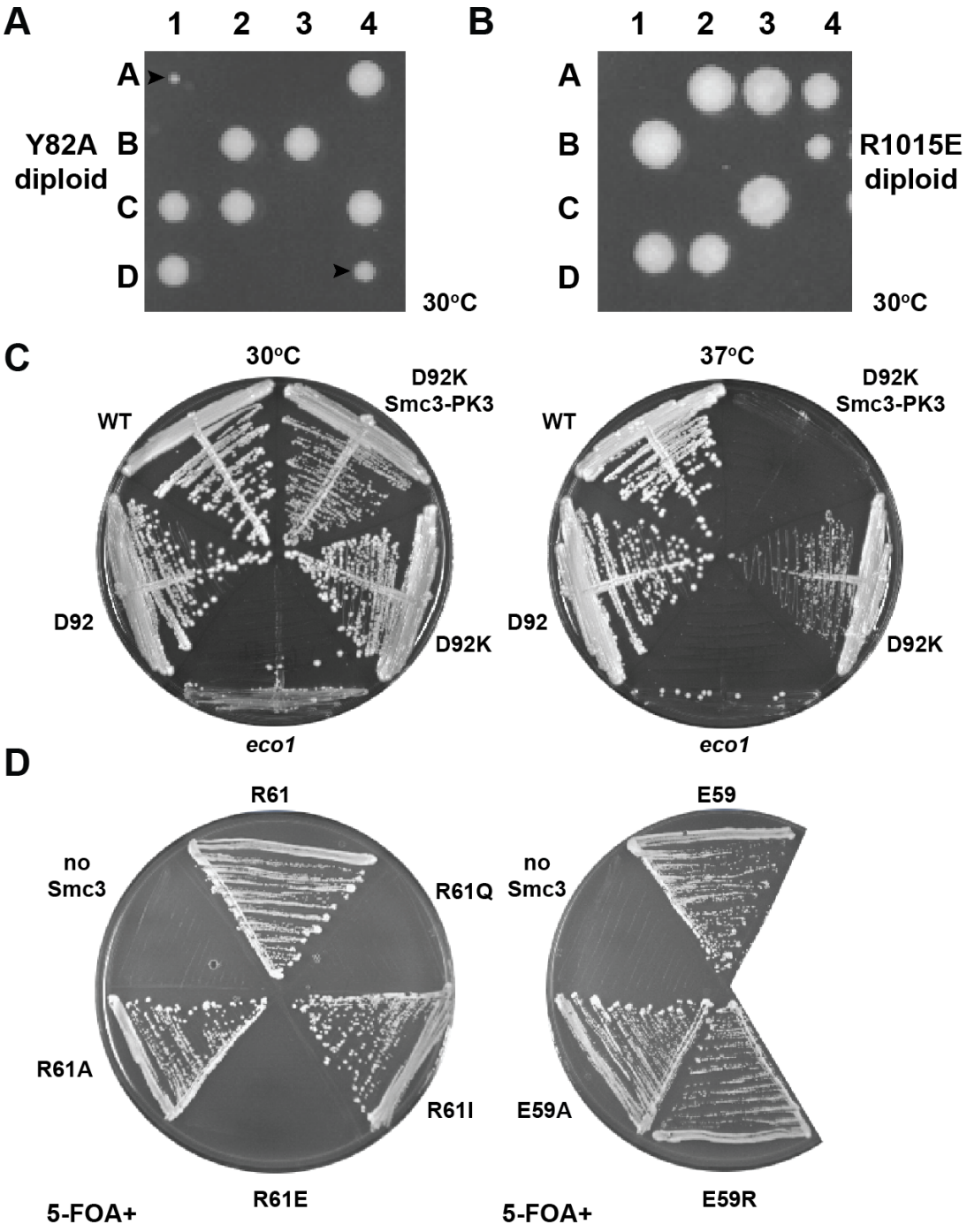
A
1 2 3 4
A
B
C
D
Y82A diploid
30°C
B
1 2 3 4
A
B
C
D
R1015E diploid
30°C
C
30°C
WT
D92K Smc3-PK3
D92
D92K
eco1
37°C
WT
D92K Smc3-PK3
D92
D92K
eco1
D
R61
no Smc3
R61Q
R61A
R61I
R61E
5-FOA+
E59
no Smc3
E59A
E59R
5-FOA+

**Figure S6.** Functional analysis of the Smc3-kleisin structure.

(A) Tetrad dissection of a diploid strain bearing *SCC1Δ* and an ectopic (single) copy of Scc1Y82A-HA6, at 30 $^{o}$C. Scc1Y82A does not fully rescue *SCC1Δ* (white arrowheads) (K23156).

(B) Tetrad dissection of a diploid strain bearing *SMC3Δ* and an ectopic (single) copy of Smc3R1015E-myc9 at 30$^{o}$C (K23110). No colonies rescuing the *SMC3Δ* were recovered.

(C) Strains bearing a single copy of Scc1D92K-HA6 grow at 30 $^{o}$C, poorly at 37 $^{o}$C, and not at all at 37$^{o}$C when combined with Smc3-PK6 (K699, K23104, K16296, K23157 and K23158).

(D) Effect of substitutions close to Smc3's KKD loop. Single copy *SMC3* genes containing E59A, E59R, R61I or R61A substitutions permit growth in the absence of a WT copy of SMC3 (5-FOA counter selection). In contrast, Smc3R61Q and R61E fail to do so (K23111-23118).

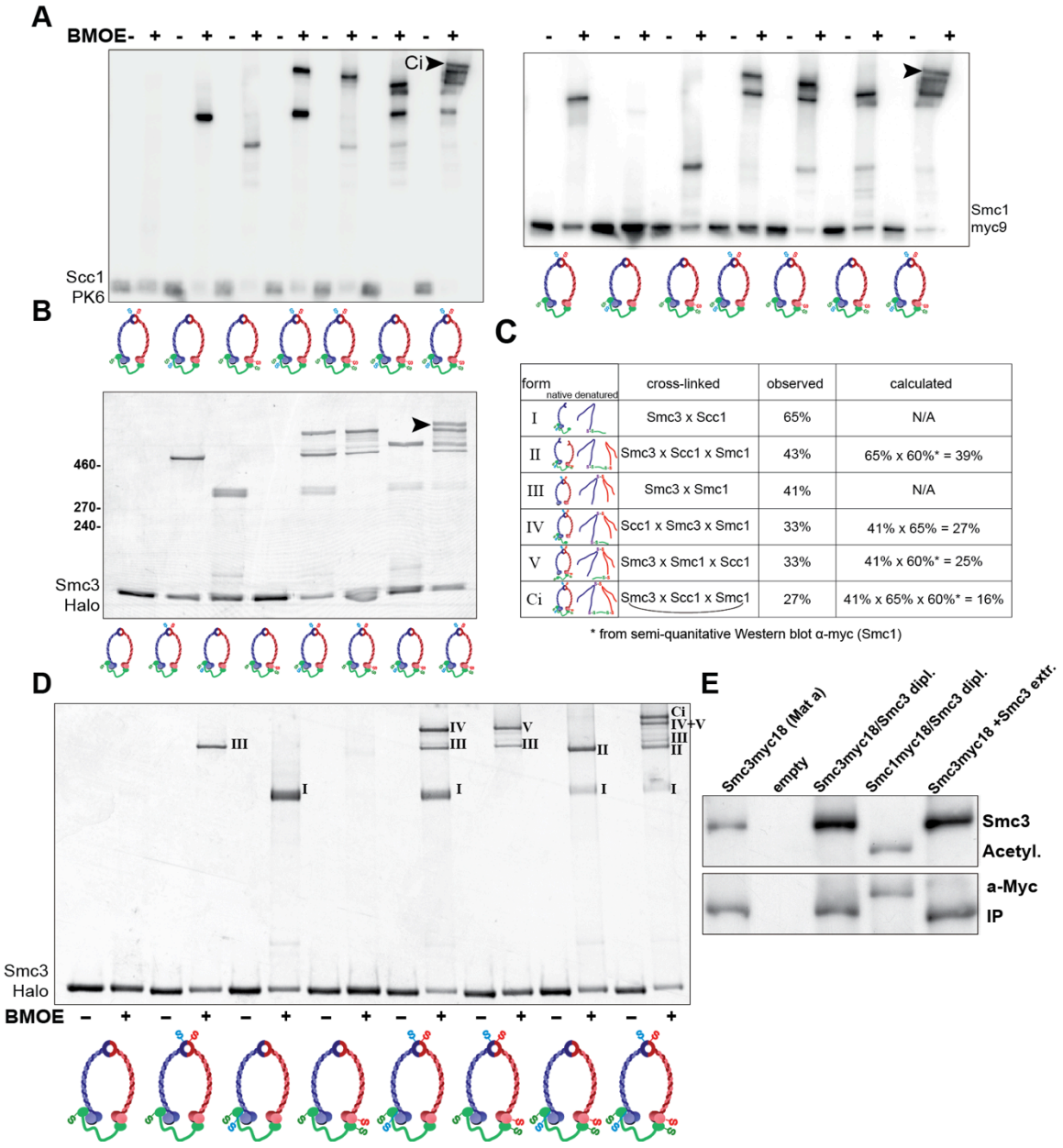
A
BMOE- + - + - + - + - + - + - +
Ci
Scc1
PK6
- + - + - + - + - + - + - +
Smc1
myc9
B
460-
270-
240-
Smc3
Halo
C
form
native denatured
cross-linked
observed
calculated
I
Smc3 x Scc1
65%
N/A
II
Smc3 x Scc1 x Smc1
43%
65% x 60%* = 39%
III
Smc3 x Smc1
41%
N/A
IV
Scc1 x Smc3 x Smc1
33%
41% x 65% = 27%
V
Smc3 x Smc1 x Scc1
33%
41% x 60%* = 25%
Ci
Smc3 x Scc1 x Smc1
27%
41% x 65% x 60%* = 16%
* from semi-quanitative Western blot α-myc (Smc1)
D
III
IV
III
V
III
II
Ci
IV+V
III
II
I
I
I
I
Smc3
Halo
BMOE – + – + – + – + – + – + – + – + – +
E
Smc3myc18 (Mat a)
empty
Smc3myc18/Smc3 dipl.
Smc1myc18/Smc3 dipl.
Smc3myc18 +Smc3 extr.
Smc3
Acetyl.
a-Myc
IP

**Figure S7.** Cohesin forms heterotrimeric rings.

(A) Immuno-precipitated Scc1-PK6 cohesin obtained after in vivo cross-linking using BMOE of strains K22013-K22020 was run on a 3-8 % Tris-acetate gel, proteins transferred by Western blotting and detected using anti-PK (Scc1, left) or anti-myc (Smc1, right).

(B) In vitro bBBR cross-linking and Smc3-Halo-TMR labeling after immuno-precipitation using anti-PK (strains K22013-K22020) showed the appearance of a slow migrating, high molecular weight form Ci (black arrowheads). Ci appeared only when all three interfaces contained cross-linkable cysteine pairs. Similar relative amounts of cross-linked dimers, linear trimers and circular trimer compared to in vivo cross-linking were observed.

(C and D) Observed and calculated in vivo cross-linking efficiencies for cohesin containing one, two or three cysteine pairs. Notice the difference on the resulting migrating species after denaturation, of open (V) and closed (Ci) cohesin trimers (first and second column). Cross-linking efficiencies were calculated from Halo-TMR fluorescence gels using AIDA image software and automated peak search over each lane. Efficiency of the Scc1-Smc1 crosslink was determined using semi-quantitative Western blot analysis of the anti-myc Western blot in (A) (LI-COR Odyssey FC).

(E) Acetylated cohesin contains a single Smc3 molecule. In diploid cells arrested in G2/M with nocodazole, protein encoded from the Smc3-myc18 allele fails to interact and co-precipitate with the WT acetylated Smc3 protein (K23159). Smc1-myc18 on the contrary can interact with WT acetylated Smc3 (K23160). Mixing extracts of two haploid strains bearing WT and myc-tagged Smc3 (last lane) does not lead to any exchange of subunits (K700, K700+K10905).

## Supplementary Tables S1-S2

**Table S1:** Crystallographic data

| | *Smc3hd:Scc1-N native* | *Smc3hd:Scc1-N SeMet* | *Smc3hd:Scc1-N(K52M) SeMet* |
|---|---|---|---|
| **Components** | Smc3hd: MA-2-261-SSKHPTSLVPRGS-971-1230-STRPII; Scc1-N: 1-115-HHHHHH; ATPγS | Smc3hd: MA-2-261-SSKHPTSLVPRGS-971-1230-STRPII; Scc1-N: 1-115-HHHHHH; ATPγS | Smc3hd: MA-2-261-SSKHPTSLVPRGS-971-1230-STRPII; Scc1-N: 1-(K52M)-115-HHHHHH; ATPγS |
| GenBank IDs | CAA89366.1; EDN60343.1 | CAA89366.1; EDN60343.1 | CAA89366.1; EDN60343.1 |
| **Data collection** | | | |
| Beamline | Diamond I24 | Diamond I02 | Diamond I03 |
| Wavelength [Å] | Se peak | Se peak | 0.97934 |
| **Crystal** | | | |
| Space group | I222 | I222 | I222 |
| Cell [Å] | 73.1, 94.8, 284.8 | 72.9, 92.9, 283.5 | 73.1, 92.0, 284.9 |
| **Scaling** | | | |
| Resolution [Å] | 3.3 | 4.0 | 4.2 |
| Number of crystals | 5 | 7 | 1 |
| Completeness [%][1] | 100.0 (100.0) | 100.0 (100.0) | 100.0 (100.0) |
| Multiplicity[1] | 25.6 (26.6) | 68.5 (65.1) | 12.9 (13.4) |
| Ano completeness [%][1] | | 100.0 (100.0) | 100.0 (100.0) |
| Ano multiplicity[1] | | 36.8 (33.8) | 7.0 (7.1) |
| Ano correlation[1, 2] | | 0.745 | 0.777 |
| $I / \sigma I$ [1] | 17.7 (2.2) | 18.0 (3.0) | 14.0 (3.5) |
| $R_{pim}$ [1] | 0.022 (0.401) | 0.027 (0.497) | 0.039 (0.311) |
| CC1/2[1, 2] | 0.999 (0.852) | 0.998 (0.925) | 0.999 (0.946) |
| **Phasing** | | | |
| Scatterer / mode | | SeMet | SeMet |
| Number of sites | | 16 | 17 |
| **Refinement** | | | |
| Model | Smc3hd: 2-81, 105-247, 975-1070, 1108-1222; 1 ATPγS; Scc1-N: 25-31, 39-102 | | |
| $R / R_{free}$ [3] | 0.274 (0.328) | | |
| Bond length rmsd [Å] | 0.011 | | |
| Bond angle rmsd [°] | 1.778 | | |
| Molprobity score | 3.2 (77th percentile) | | |
| Favoured [%][4] | 96.2 | | |
| Disallowed [%][4] | 0.6 | | |
| **PDB ID** | **4UX3** | | |

[1] Values in parentheses refer to the highest recorded resolution shell.
[2] Correlation coefficient between half sets (CCP4 SCALA).
[3] 5 % of reflections were randomly selected before any refinement.
[4] Percentage of residues in Ramachandran plot areas (CCP4 PROCHECK).

**Table S2:** List of yeast strains used in this study

| Strain Number | Genotype (Mutations common to all strains are not indicated but all strains are derivatives of strains K699/K700) |
|---|---|
| K699 | MATa, *ade2-1*, *trp1-1*, *can1-100*, *leu2-3*,112,*his3-11,15*, URA3, GAL, psi+ |
| K700 | MATα, *ade2-1*, *trp1-1*, *can1-100*, *leu2-3*,112,*his3-11,15*, URA3, GAL, psi+ |
| K10905 | MATa, *SMC3-MYC18*::URA3 |
| K16296 | MATα , *ade2-1*, *trp1-1*, *can1-100*, *leu2-3*,112,*his3-11,15*, URA3, GAL, psi+ *eco1-1*(G211D) |
| K17309 | MATa, GAL-*SCC1*Myc18, *scc1*::URA3, *SMC3*-PK6::KanMX4, pLH157 (TRP1+), YEpLac181-p*SCC1-SCC1*HA6 WT |
| K17106 | MATa, GAL-*SCC1*Myc18, *scc1*::URA3, *SMC3*-PK6::KanMX4, pLH157 (TRP1+), YEpLac181-p*SCC1-SCC1*HA6 T3stop(TAG) |
| K17310 | MATa, GAL-*SCC1*Myc18, *scc1*::URA3, *SMC3*-PK6::KanMX4, pLH157 (TRP1+), YEpLac181-p*SCC1-SCC1*HA6 W25stop(TAG) |
| K17311 | MATa, GAL-*SCC1*Myc18, *scc1*::URA3, *SMC3*-PK6::KanMX4, pLH157 (TRP1+), YEpLac181-p*SCC1-SCC1*HA6 N5stop(TAG) |
| K17312 | MATa, GAL-*SCC1*Myc18, *scc1*::URA3, *SMC3*-PK6::KanMX4, pLH157 (TRP1+), YEpLac181-p*SCC1-SCC1*HA6 R8stop(TAG) |
| K17316 | MATa, GAL-*SCC1*Myc18, *scc1*::URA3, *SMC3*-PK6::KanMX4, pLH157 (TRP1+), YEpLac181-p*SCC1-SCC1*HA6 I100stop(TAG) |
| K17540 | MATa, GAL-*SCC1*Myc18, *scc1*::URA3, *SMC3*-PK6::KanMX4, pLH157 (TRP1+), YEpLac181-p*SCC1-SCC1*HA6 P6stop(TAG) |
| K18806 | MATa, *leu2*:*SCC1*-HA6::hphNT1::*leu2*, *scc1*::KanMX4 |
| K19447 | MATa, *leu2*:*SCC1*(Q76C)-HA6::hphNT1::*leu2*, *scc1*::KanMX4 |
| K19579 | MATa, *his3*:*SMC3*(E188C)-MYC9::natNT2::*his3*, *smc3*::HIS3MX, *leu2*:*SCC1*(Q76C)-HA6::hphNT1::*leu2*, *scc1*::KanMX4 |
| K19724 | MATa, *his3*:*SMC3*(E174C)-MYC9::natNT2::*his3*, *smc3*::HIS3MX, *leu2*:*SCC1*(Q76C)-HA6::hphNT1::*leu2*, *scc1*::KanMX4 |
| K19727 | MATa, *his3*:*SMC3*(A181C)-MYC9::natNT2::*his3*, *smc3*::HIS3MX, *leu2*:*SCC1*(Q76C)-HA6::hphNT1::*leu2*, *scc1*::KanMX4 |
| K19728 | MATa, *his3*:*SMC3*(K185C)-MYC9::natNT2::*his3*, *smc3*::HIS3MX, *leu2*:*SCC1*(Q76C)-HA6::hphNT1::*leu2*, *scc1*::KanMX4 |
| K19732 | MATa, *his3*:*SMC3*(K185C)-MYC9::natNT2::*his3*, *smc3*::HIS3MX, *leu2*:*SCC1*(R80C)-HA6::hphNT1::*leu2*, *scc1*::KanMX4 |
| K19764 | MATα, *his3*:*SMC3*(S1043C)-MYC9::natNT2::*his3*, *smc3*::HIS3MX, *leu2*:*SCC1*-HA6::hphNT1::*leu2*, *scc1*::KanMX4 |
| K19769 | MATα, *his3*:*SMC3*(S174C)-MYC9::natNT2::*his3*, *smc3*::HIS3MX, *leu2*:*SCC1*(R69C)-HA6::hphNT1::*leu2*, *scc1*::KanMX4 |
| K19796 | MATa, *his3*:*SMC3*-MYC9::natNT2::*his3*, *smc3*::HIS3MX, *leu2*:*SCC1*-HA6::hphNT1::*leu2*, *scc1*::KanMX4 |
| K20279 | MATa, *leu2*: *SMC1*(G22C,K639C)-MYC9::hphNT1::*leu2*, *SMC1*::NatMX4, *SCC1*(A547C)-PK6::KanMX4, *SMC3*(E570C,S1043C)-HA6::HIS3MX, 2.3kb TRP1-Cen4-ARS1 minichromosome |
| K20280 | MATa, *leu2*: *SMC1*(G22C,K639C)-MYC9::hphNT1::*leu2*, *SMC1*::NatMX4, *SCC1*-PK6::KanMX4, *SMC3*(E570C,S1043C)-HA6::HIS3MX, 2.3kb TRP1-Cen4-ARS1 minichromosome |
| K20300 | MATa, *leu2*: *SMC1*(G22C,K639C)-MYC9::hphNT1::*leu2*, *SMC1*::NatMX4, *SCC1*(C56S, A547C)-PK6::KanMX4, *SMC3*(E570C,S1043C)-HA6::HIS3MX, 2.3kb TRP1-Cen4-ARS1 minichromosome |
| K20355 | MATa, *his3*:*SMC3*-MYC9::natNT2::*his3*, *SMC3*::HIS3MX, *leu2*:*SCC1*-HA6::hphNT1::*leu2*, *scc1*::KanMX4, *trp1*::*SMC1*::TRP1 |
| K20356 | MATa, *his3*:*SMC3*(A181C)-MYC9::natNT2::*his3*, *smc3*::HIS3MX, *leu2*:*SCC1*(Q76C)- |

| | |
|---|---|
| | HA6::hphNT1::*leu2*, *scc1*::KanMX4, *trp1*::*SMC1*::TRP1 |
| K20357 | MATa, *his3*:*SMC3*(A181C, L1029R)-MYC9::natNT2::*his3*, *smc3*::HIS3MX, *leu2*:*SCC1*(Q76C)-HA6::hphNT1::*leu2*, *scc1*::KanMX4, *trp1*::*SMC1*::TRP1 |
| K20358 | MATa, *SCC1*-PK6::KanMX4, *smc3*::HIS3MX, pLH157, YCpLac33-*SMC3*-MYC9, YEpLac181-*SMC3*-HA3 |
| K20359 | MATa, *SCC1*-PK6::KanMX4, *smc3*::HIS3MX, pLH157, YCpLac33-*smc3*-MYC9, YEpLac181-*smc3*(A181*amber*)-HA3 |
| K20360 | MATa, *SCC1*-PK6::KanMX4, *smc3*::HIS3MX, pLH157, YCpLac33-*SMC3*-MYC9, YEpLac181-*SMC3*(K185*amber*)-HA3 |
| K20361 | MATa, *SCC1*-PK6::KanMX4, *smc3*::HIS3MX, pLH157, YCpLac33-*SMC3*-MYC9, YEpLac181-*SMC3*(K206*amber*)-HA3 |
| K20362 | MATa, *SCC1*-PK6::KanMX4, *smc3*::HIS3MX, pLH157, YCpLac33-*SMC3*-MYC9, YEpLac181-*SMC3*(K1018*amber*)-HA3 |
| K20363 | MATa, *SCC1*-PK6::KanMX4, *smc3*::HIS3MX, pLH157, YCpLac33-*SMC3*-MYC9, YEpLac181-*SMC3*(A1040*amber*)-HA3 |
| K20364 | MATa, *SCC1*-PK6::KanMX4, *smc3*::HIS3MX, pLH157, YCpLac33-*SMC3*-MYC9, YEpLac181-*SMC3*(E1050*amber*)-HA3 |
| K20366 | MATa, *smc3*::HIS3MX, Nmyc9-*SCC1*(Met1Ile, Met30Ile), YEpLac181-*SMC3*-HA3, pLH157 |
| K20367 | MATa, *smc3*::HIS3MX, Nmyc9-*SCC1*(Met1Ile, Met30Ile), YEpLac181-*SMC3*(A181*amber*)-HA3, pLH157 |
| K22013 | MATα, *leu2*:*SMC1*-MYC9::hphNT1::*leu2*, *SMC1*::NatMX4, *SCC1*-PK6::KanMX4, *SMC3*-Halo::ADE2 |
| K22014 | MATα, *leu2*:*SMC1*(K639C)-MYC9::hphNT1::*leu2*, *SMC1*::NatMX4, *SCC1*-PK6::KanMX4, *SMC3*(E570C)-Halo::ADE2 |
| K22015 | MATa, *leu2*:*SMC1*-MYC9::hphNT1::*leu2*, *SMC1*::NatMX4, *SCC1*-PK6::KanMX4, *SMC3*(S1043C)-Halo::ADE2 |
| K22016 | MATα, *leu2*:*SMC1*(K639C)-MYC9::hphNT1::*leu2*, *SMC1*::NatMX4, *SCC1*-PK6::KanMX4, *SMC3*(E570C,S1043C)-Halo::ADE2 |
| K22017 | MATα, *leu2*:*SMC1*(G22C)-MYC9::hphNT1::*leu2*, *SMC1*::NatMX4, *SCC1*(A547C)-PK6::KanMX4, *SMC3*-Halo::ADE2 |
| K22018 | MATa, *leu2*:*SMC1*(G22C,K639C)-MYC9::hphNT1::*leu2*, *SMC1*::NatMX4, *SCC1*(A547C)-PK6::KanMX4, *SMC3*(E570C)-Halo::ADE2 |
| K22019 | MATa, *leu2*:*SMC1*(G22C,K639C)-MYC9::hphNT1::*leu2*, *SMC1*::NatMX4, *SCC1*(A547C)-PK6::KanMX4, *SMC3*(E570C,S1043C)-Halo::ADE2 |
| K22020 | MATa, *leu2*:*SMC1*(G22C)-MYC9::hphNT1::*leu2*, *SMC1*::NatMX4, *SCC1*(A547C)-PK6::KanMX4, *SMC3*(S1043C))-Halo::ADE2 |
| K22590 | MATa,/α, *leu2*:*SMC1*(G22C,K639C)-MYC9::hphNT1::*leu2*/ *leu2*:*SMC1*(G22C,K639C)-MYC9::hphNT1::*leu2*, *SMC1*::NatMX4/*SMC1*::NatMX4, *SCC1*(A547C)-PK6::KanMX4/*SCC1*(A547C)-PK6::KanMX4, *SMC3*(E570C,S1043C)-Halo::ADE2/*SMC3*(E570C,S1043C)-HA6::HIS3MX |
| K23102 | MATa, *his3*:*SMC3*(K1032C)-MYC9::natNT2::*his3*, *SMC3*::HIS3MX, *leu2*:*SCC1*(C56S K48C)-HA6::hphNT1::*leu2*, *scc1*::KanMX4 |
| K23103 | MATa, *his3*:*SMC3*(F1005C)-MYC9::natNT2::*his3*, *SMC3*::HIS3MX, *leu2*:*SCC1*(I100C)-HA6::hphNT1::*leu2*, *scc1*::KanMX4 |
| K23104 | MATa, *leu2*:*SCC1*-HA6::hphNT1::*leu2*, *scc1*::KanMX4 |
| K23105 | MATa, *leu2*:*SCC1*(Y82A)-HA6::hphNT1::*leu2*, *scc1*::KanMX4, spore 12D |
| K23106 | MATa, *leu2*:*SCC1*(Y82A)-HA6::hphNT1::*leu2*, *scc1*::KanMX4, spore 5D |
| K23107 | MATa,/α *leu2*::*SMC3*GFP::LEU2 Mtw1-RFP:KanMX4 *SMC1*myc9::URA3 *leu2*::*SCC1*HA6:hphNT1/*leu2*::*SMC3*GFP::LEU2 Mtw1-RFP:KanMX4 *SMC1*myc9::URA3 *leu2*::*SCC1*HA6::hphNT1 |
| K23108 | MATa,/α *leu2*::*SMC3*(L1029R)GFP::LEU2 Mtw1-RFP:KanMX4 *SMC1*myc9::URA3 *leu2*::*SCC1*HA6:hphNT1/*leu2*::*SMC3*(L1029R)GFP::LEU2 Mtw1-RFP:KanMX4 *SMC1*myc9::URA3 *leu2*::*SCC1*HA6::hphNT1 |
| K23109 | MATa,/α *leu2*::*SMC3*(R61Q)GFP::LEU2 Mtw1-RFP:KanMX4 *SMC1*myc9::URA3 |

| | |
|---|---|
| | *leu2*::*SCC1*HA6:hphNT1/*leu2*::*SMC3*(R61Q)GFP::LEU2 Mtw1- RFP:KanMX4 *SMC1*myc9::URA3 *leu2*::*SCC1*HA6::hphNT1RFP:KanMX4 *SMC1*myc9::URA3 *leu2*::*SCC1*HA6::hphNT1 |
| K23110 | MATa,/α, *his3*:*SMC3*(R1015E)-MYC9::natNT2::*his3*, *SMC3*::HIS3MX |
| K23111 | MATa,*smc3*::hphNT1 *his3*:natNT2::*his3* + YCpLac33-*SMC3*myc9 |
| K23112 | MATa,*smc3*::hphNT1 *his3*:*SMC3*-MYC9:natNT2::*his3*,YCpLac33-*SMC3*myc9 |
| K23113 | MATa, *smc3*::hphNT1 *his3*:*SMC3*(R61I)-MYC9::natNT2::*his3*,YCpLac33-*SMC3*myc9 |
| K23114 | MATa, *smc3*::hphNT1 *his3*:*SMC3*(R61Q)-MYC9::natNT2::*his3*,YCpLac33-*SMC3*myc9 |
| K23115 | MATa, *smc3*::hphNT1 *his3*:*SMC3*(R61A)-MYC9::natNT2::*his3*,YCpLac33-*SMC3*myc9 |
| K23116 | MATa, *smc3*::hphNT1 *his3*:*SMC3*(R61E)-MYC9::natNT2::*his3*,YCpLac33-*SMC3*myc9 |
| K23117 | MATa, *smc3*::hphNT1 *his3*:*SMC3*(E59A)-MYC9::natNT2::*his3*, YCpLac33-*SMC3*myc9 |
| K23118 | MATa, *smc3*::hphNT1 *his3*:*SMC3*(E59R)-MYC9::natNT2::*his3*,YCpLac33-*SMC3*myc9 |
| K23119 | MATa, *scc1*::NatMX4 , *leu2*:*SCC1*R69E)-HA6::hphNT1::*leu2* |
| K23120 | MATa, *scc1*::NatMX4 , *leu2*:*SCC1*(R69A)-HA6::hphNT1::*leu2* |
| K23121 | MATa, *SMC3*::hphNT1 *his3*:*SMC3*(E1000A)-MYC9::natNT2::*his3*,YCpLac33-*SMC3*myc9 |
| K23122 | MATa, *smc3*::hphNT1 *his3*:*SMC3*(F1005A)-MYC9::natNT2::*his3*,YCpLac33-*SMC3*myc9 |
| K23123 | MATa, *smc3*::hphNatMX4 *his3*:*SMC3*(R1008A)-MYC9::natNT2::*his3*,YCpLac33-*SMC3*myc9 |
| K23124 | MATa, *smc3*::hphMX*4 his3*:*SMC3*(R1009A)-MYC9::natNT2::*his3*,YCpLac33-*SMC3*myc9 |
| K23125 | MATa, *smc3*::hphMX4 *his3*:*SMC3*(L1029R)-MYC9::natNT2::*his3*,YCpLac33-*SMC3*myc9 |
| K23126 | MATa, *smc3*::hphMX*4 his3*:*SMC3*(I1026R)-MYC9::natNT2::*his3*,YCpLac33-*SMC3*myc9 |
| K23127 | MATa, *smc3*::hphMX4 *his3*:*SMC3*(L1029R)-MYC9::natNT2::*his3*,YCpLac33-*SMC3*myc9 |
| K23128 | MATa, *his3*:*SMC3*(S1043C)-MYC9::natNT2::*his3*, *smc3*::HIS3MX, *leu2*:*SCC1*-HA6::hphNT1::*leu2*, *scc1*::KanMX4, *trp1*::*SMC1*::TRP1 |
| K23129 | MATa, *his3*:*SMC3*(S1043C,L1029R)-MYC9::natNT2::*his3*, *smc3*::HIS3MX, *leu2*:*SCC1*-HA6::hphNT1::*leu2*, *scc1*::KanMX4, *trp1*::*SMC1*::TRP1 |
| K23130 | MATa, *smc3*::HIS3MX *his3*:*SMC3*(S1043C)-MYC9::natNT2::*his3*, ,*leu2*:*SCC1*-HA6::hphNT1::*leu2* |
| K23131 | MATa, *smc3*::HIS3MX *his3*:*SMC3*(S1043C)-MYC9::natNT2::*his3*, ,*leu2*:*SCC1*(L89K)-HA6::hphNT1::*leu2* |
| K23132 | MATa,/α *his3*:*SMC3*hphMX4, , *his3*:*SMC3*(K206E)-MYC9::natNT2::*his3* |
| K23133 | MATa,/α *his3*:*SMC3*hphMX4, , *his3*:*SMC3*(E216A)-MYC9::natNT2::*his3* |
| K23134 | MATa, *smc3*::hphMX4 *his3*:*SMC3*(K996A)-MYC9::natNT2::*his3*,YCpLac33-*SMC3*myc9 |
| K23135 | MATa, *smc3*::hphMX4 *his3*:*SMC3*(K996D)-MYC9::natNT2::*his3*,YCpLac33-*SMC3*myc9 |
| K23136 | MATa, *scc1*::NatMX4 , *leu2*:*SCC1*(Y82I)-HA6::hphNT1::leu2, *scc1*::KanMX4 |
| K23137 | MATa, *scc1*::NatMX4 , *leu2*:*SCC1*(Y82F)-HA6::hphNT1::leu2, *scc1*::KanMX4 |
| K23138 | MATa, *scc1*::NatMX4 , *leu2*::hphNT1::leu2, YCpLac33-*pSCC1-SCC1* |
| K23139 | MATa, *scc1*::NatMX4 , *leu2*:: *SCC1*-HA6hphNT1::leu2, YCpLac33-*pSCC1-SCC1* |
| K23140 | MATa, *scc1*::NatMX4 , *leu2*:*SCC1*(D95K)-HA6::hphNT1::leu2, YCpLac33-*pSCC1-SCC1* |
| K23141 | MATa, *scc1*::NatMX4 , *leu2*:*SCC1*(K99D)-HA6::hphNT1::leu2, YCpLac33-*pSCC1-SCC1* |
| K23142 | MATa, *scc1*::NatMX4 , *leu2*:*SCC1*(K99A)-HA6::hphNT1::leu2, YCpLac33-*pSCC1-SCC1* |
| K23143 | MATa,/α *scc1*::NatMX4 , *leu2*:*SCC1*(D95A,K99A)-HA6::hphNT1::*leu2, SMC3*-PK6 |
| K23146 | MATa, *his3*:*SMC3*-MYC9::natNT2::*his3*, *smc3*::HIS3MX, *leu2*:*SCC1*- |

| | |
|---|---|
| | HA6::hphNT1::*leu2*, *scc1*::KanMX4, *trp1*::*SMC1*::TRP1 |
| K23147 | MATa, *SCC1*-HA6::HIS3MX, *SMC1*-PK6::KanMX6, *his3*::natNT2::*his3* |
| K23148 | MATa, *SCC1*-HA6::HIS3MX, *SMC1*-PK6::KanMX6, *his3*:SMC3-MYC9:natNT2::*his3* |
| K23149 | MATa, *SCC1*-HA6::HIS3MX, *SMC1*-PK6::KanMX6, *his3*:*SMC3*(R1009A)-MYC9::natNT2::*his3* |
| K23150 | MATa, *SCC1*-HA6::HIS3MX, *SMC1*-PK6::KanMX6, *his3*:*SMC3*(L1019R)-MYC9::natNT2::*his3* |
| K23151 | MATa, *SCC1*-HA6::HIS3MX, *SMC1*-PK6::KanMX6, *his3*:*SMC3*(I1026R)-MYC9::natNT2::*his3* |
| K23152 | MATa, *SCC1*-HA6::HIS3MX, *SMC1*-PK6::KanMX6, *his3*:*SMC3*(L1029R)-MYC9::natNT2::*his3* |
| K23153 | MATa, *SCC1*-PK6::KanMX4, pLH157, YEpLac181-*SMC3*-HA3 |
| K23154 | MATa, *SCC1*-PK6::KanMX4, pLH157, YEpLac181-*SMC3*A181*amber*-HA3 |
| K23155 | MATa, *SCC1*-PK6::KanMX4, pLH157, YEpLac181-*SMC3*A181*amber*,L1029R-HA3 |
| K23156 | MATa,/α *scc1*::NatMX4 , *leu2*:*SCC1*(Y82A)-HA6::hphNT1::*leu2, SMC3*-PK6::KanMX6 |
| K23157 | MATa, *scc1*::NatMX4 , *leu2*:*SCC1*(D92K)-HA6::hphNT1::*leu2* |
| K23158 | MATa, *scc1*::NatMX4 , *leu2*:*SCC1*(D92K)-HA6::hphNT1::*leu2, SMC3*-PK6::KanMX6 |
| K23159 | MATa,/α *SMC3-MYC18*::URA3 |
| K23160 | MATa,/α *SMC1-MYC18*::URA3 |

**References and Notes**


1. J. M. Peters, A. Tedeschi, J. Schmitz, The cohesin complex and its roles in chromosome biology. *Genes Dev.* **22**, 3089–3114 (2008). Medline doi:10.1101/gad.1724308

2. K. Nasmyth, Cohesin: A catenase with separate entry and exit gates? *Nat. Cell Biol.* **13**, 1170–1177 (2011). Medline doi:10.1038/ncb2349

3. S. Gruber, C. H. Haering, K. Nasmyth, Chromosomal cohesin forms a ring. *Cell* **112**, 765–777 (2003). Medline doi:10.1016/S0092-8674(03)00162-4

4. C. H. Haering, J. Löwe, A. Hochwagen, K. Nasmyth, Molecular architecture of SMC proteins and the yeast cohesin complex. *Mol. Cell* **9**, 773–788 (2002). Medline doi:10.1016/S1097-2765(02)00515-4

5. S. Gruber, P. Arumugam, Y. Katou, D. Kuglitsch, W. Helmhart, K. Shirahige, K. Nasmyth, Evidence that loading of cohesin onto chromosomes involves opening of its SMC hinge. *Cell* **127**, 523–537 (2006). Medline doi:10.1016/j.cell.2006.08.048

6. K. L. Chan, M. B. Roig, B. Hu, F. Beckouët, J. Metson, K. Nasmyth, Cohesin's DNA exit gate is distinct from its entrance gate and is regulated by acetylation. *Cell* **150**, 961–974 (2012). Medline doi:10.1016/j.cell.2012.07.028

7. K. L. Chan, T. Gligoris, W. Upcher, Y. Kato, K. Shirahige, K. Nasmyth, F. Beckouët, Pds5 promotes and protects cohesin acetylation. *Proc. Natl. Acad. Sci. U.S.A.* **110**, 13020–13025 (2013). Medline doi:10.1073/pnas.1306900110

8. F. Bürmann, H. C. Shin, J. Basquin, Y. M. Soh, V. Giménez-Oya, Y. G. Kim, B. H. Oh, S. Gruber, An asymmetric SMC-kleisin bridge in prokaryotic condensin. *Nat. Struct. Mol. Biol.* **20**, 371–379 (2013). Medline doi:10.1038/nsmb.2488

9. C. H. Haering, A. M. Farcas, P. Arumugam, J. Metson, K. Nasmyth, The cohesin ring concatenates sister DNA molecules. *Nature* **454**, 297–301 (2008). Medline doi:10.1038/nature07098

10. A. Schleiffer, S. Kaitna, S. Maurer-Stroh, M. Glotzer, K. Nasmyth, F. Eisenhaber, Kleisins: A superfamily of bacterial and eukaryotic SMC protein partners. *Mol. Cell* **11**, 571–575 (2003). Medline doi:10.1016/S1097-2765(03)00108-4

11. P. Arumugam, T. Nishino, C. H. Haering, S. Gruber, K. Nasmyth, Cohesin's ATPase activity is stimulated by the C-terminal Winged-Helix domain of its kleisin subunit. *Curr. Biol.* **16**, 1998–2008 (2006). Medline doi:10.1016/j.cub.2006.09.002

12. B. Hu, T. Itoh, A. Mishra, Y. Katoh, K. L. Chan, W. Upcher, C. Godlee, M. B. Roig, K. Shirahige, K. Nasmyth, ATP hydrolysis is required for relocating cohesin from sites occupied by its Scc2/4 loading complex. *Curr. Biol.* **21**, 12–24 (2011). Medline doi:10.1016/j.cub.2010.12.004

13. E. Unal, J. M. Heidinger-Pauli, W. Kim, V. Guacci, I. Onn, S. P. Gygi, D. E. Koshland, A molecular determinant for the establishment of sister chromatid cohesion. *Science* **321**, 566–569 (2008). Medline doi:10.1126/science.1157880

14. T. Rolef Ben-Shahar, S. Heeger, C. Lehane, P. East, H. Flynn, M. Skehel, F. Uhlmann, Eco1-dependent cohesin acetylation during establishment of sister chromatid cohesion. *Science* **321**, 563–566 (2008). Medline doi:10.1126/science.1157774

15. B. D. Rowland, M. B. Roig, T. Nishino, A. Kurze, P. Uluocak, A. Mishra, F. Beckouët, P. Underwood, J. Metson, R. Imre, K. Mechtler, V. L. Katis, K. Nasmyth, Building sister chromatid cohesion: Smc3 acetylation counteracts an antiestablishment activity. *Mol. Cell* **33**, 763–774 (2009). Medline doi:10.1016/j.molcel.2009.02.028

16. F. Beckouët, B. Hu, M. B. Roig, T. Sutani, M. Komata, P. Uluocak, V. L. Katis, K. Shirahige, K. Nasmyth, An Smc3 acetylation cycle is essential for establishment of sister chromatid cohesion. *Mol. Cell* **39**, 689–699 (2010). Medline doi:10.1016/j.molcel.2010.08.008

17. T. Sutani, T. Kawaguchi, R. Kanno, T. Itoh, K. Shirahige, Budding yeast Wpl1(Rad61)-Pds5 complex counteracts sister chromatid cohesion-establishing reaction. *Curr. Biol.* **19**, 492–497 (2009). Medline doi:10.1016/j.cub.2009.01.062

18. C. E. Huang, M. Milutinovich, D. Koshland, Rings, bracelet or snaps: Fashionable alternatives for Smc complexes. *Philos. Trans. R. Soc. London B Biol. Sci.* **360**, 537–542 (2005). Medline doi:10.1098/rstb.2004.1609

19. D. Ivanov, K. Nasmyth, A physical assay for sister chromatid cohesion in vitro. *Mol. Cell* **27**, 300–310 (2007). Medline doi:10.1016/j.molcel.2007.07.002

20. C. H. Haering, D. Schoffnegger, T. Nishino, W. Helmhart, K. Nasmyth, J. Löwe, Structure and stability of cohesin's Smc1-kleisin interaction. *Mol. Cell* **15**, 951–964 (2004). Medline doi:10.1016/j.molcel.2004.08.030

21. A. Kurze, K. A. Michie, S. E. Dixon, A. Mishra, T. Itoh, S. Khalid, L. Strmecki, K. Shirahige, C. H. Haering, J. Löwe, K. Nasmyth, A positively charged channel within the Smc1/Smc3 hinge required for sister chromatid cohesion. *EMBO J.* **30**, 364–378 (2011). Medline doi:10.1038/emboj.2010.315

22. F. Uhlmann, F. Lottspeich, K. Nasmyth, Sister-chromatid separation at anaphase onset is promoted by cleavage of the cohesin subunit Scc1. *Nature* **400**, 37–42 (1999). Medline doi:10.1038/21831

23. S. B. Buonomo, R. K. Clyne, J. Fuchs, J. Loidl, F. Uhlmann, K. Nasmyth, Disjunction of homologous chromosomes in meiosis I depends on proteolytic cleavage of the meiotic cohesin Rec8 by separin. *Cell* **103**, 387–398 (2000). Medline doi:10.1016/S0092-8674(00)00131-8

24. A. Losada, M. Hirano, T. Hirano, Identification of Xenopus SMC protein complexes required for sister chromatid cohesion. *Genes Dev.* **12**, 1986–1997 (1998). Medline doi:10.1101/gad.12.13.1986

25. I. Sumara, E. Vorlaufer, C. Gieffers, B. H. Peters, J.-M. Peters, Characterization of vertebrate cohesin complexes and their regulation in prophase. *J. Cell Biol.* **151**, 749–762 (2000). Medline doi:10.1083/jcb.151.4.749

26. R. Gandhi, P. J. Gillespie, T. Hirano, Human Wapl is a cohesin-binding protein that promotes sister-chromatid resolution in mitotic prophase. *Curr. Biol.* **16**, 2406–2417 (2006). Medline doi:10.1016/j.cub.2006.10.061

27. S. Kueng, B. Hegemann, B. H. Peters, J. J. Lipp, A. Schleiffer, K. Mechtler, J. M. Peters, Wapl controls the dynamic association of cohesin with chromatin. *Cell* **127**, 955–967 (2006). Medline doi:10.1016/j.cell.2006.09.040

28. M. B. Roig , J. Löwe , K. L. Chan, F. Beckouët, J. Metson, K. Nasmyth, Structure and function of cohesin's Scc3/SA regulatory subunit. *FEBS Lett.* **16**, 3692–3702 (2014).

29. H. T. Chen, L. Warfield, S. Hahn, The positions of TFIIF and TFIIE in the RNA polymerase II transcription preinitiation complex. *Nat. Struct. Mol. Biol.* **14**, 696–703 (2007). Medline doi:10.1038/nsmb1272

30. A. M. Farcas, P. Uluocak, W. Helmhart, K. Nasmyth, Cohesin’s concatenation of sister DNAs maintains their intertwining. *Mol. Cell* **44**, 97–107 (2011). Medline doi:10.1016/j.molcel.2011.07.034

31. D. Stock, O. Perisic, J. Löwe, Robotic nanolitre protein crystallisation at the MRC Laboratory of Molecular Biology. *Prog. Biophys. Mol. Biol.* **88**, 311–327 (2005). Medline doi:10.1016/j.pbiomolbio.2004.07.009

32. W. Kabsch, Integration, scaling, space-group assignment and post-refinement. *Acta Crystallogr. D Biol. Crystallogr.* **66**, 133–144 (2010). Medline doi:10.1107/S0907444909047374

33. M. D. Winn, C. C. Ballard, K. D. Cowtan, E. J. Dodson, P. Emsley, P. R. Evans, R. M. Keegan, E. B. Krissinel, A. G. Leslie, A. McCoy, S. J. McNicholas, G. N. Murshudov, N. S. Pannu, E. A. Potterton, H. R. Powell, R. J. Read, A. Vagin, K. S. Wilson, Overview of the CCP4 suite and current developments. *Acta Crystallogr. D Biol. Crystallogr.* **67**, 235–242 (2011). Medline doi:10.1107/S0907444910045749

34. A. J. McCoy, R. W. Grosse-Kunstleve, P. D. Adams, M. D. Winn, L. C. Storoni, R. J. Read, Phaser crystallographic software. *J. Appl. Cryst.* **40**, 658–674 (2007). Medline doi:10.1107/S0021889807021206

35. D. Turk, MAIN software for density averaging, model building, structure refinement and validation. *Acta Crystallogr. D Biol. Crystallogr.* **69**, 1342–1357 (2013). Medline doi:10.1107/S0907444913008408

36. G. N. Murshudov, A. A. Vagin, E. J. Dodson, Refinement of macromolecular structures by the maximum-likelihood method. *Acta Crystallogr. D Biol. Crystallogr.* **53**, 240–255 (1997). Medline doi:10.1107/S0907444996012255